A Theoretical Study of the Bonding Properties of Thermoelectric R_4Sb_3 Compounds

Vincent Pelletier,[a] Hugo Bouteiller,[bc] Bruno Fontaine,[a] David Berthebaud,[d] Jean-Claude Crivello,[e] Franck Gascoin,[b] Takao Mori,[fg] Jean-François Halet,[a] and Régis Gautier*[a]

[a] *Univ Rennes, École Nationale Supérieure de Chimie de Rennes, CNRS, ISCR UMR 6226, 35000 Rennes, France*

[b] *Laboratoire CRISMAT UMR 6508 CNRS ENSICAEN, 6 boulevard du Maréchal Juin, 14050 Caen Cedex 04, France*

[c] *Materials Science and Technology Division, Oak Ridge National Laboratory, Oak Ridge, Tennessee 37831, United States*

[d] *Nantes Université, CNRS, Institut des Matériaux Jean Rouxel, 44000 Nantes, France*

[e] *CNRS-Saint Gobain-NIMS, UMI 3629, Laboratory for Innovative Key Materials and Structures (LINK), National Institute for Materials Science, Tsukuba 305-0044, Japan.*

[f] *International Center for Materials Nanoarchitectonics (MANA), National Institute for Materials Science (NIMS), Namiki 1-1, Tsukuba 305-0044, Japan*

[g] *Graduate School of Pure and Applied Sciences, University of Tsukuba, 1-1-1 Tennodai, Tsukuba, Ibaraki 305-8577, Japan*

Abstract

This study investigates the electronic structure and bonding properties of rare-earth antimonide compounds, specifically Yb_4Sb_3 and La_4Sb_3, utilizing density functional theory calculations. The research aims to elucidate the differences in thermoelectric performance between these materials, which are considered for high-temperature applications. The analysis reveals that Yb_4Sb_3 exhibits a predominantly ionic character with divalent ytterbium, leading to p-type conduction at high temperatures. In contrast, La_4Sb_3 displays more covalent bonding and n-type conduction. The study also explores the challenges of doping Yb_4Sb_3 with trivalent rare-earth atoms, a process crucial for enhancing its thermoelectric efficiency. The findings provide insights into the structural and electronic properties that govern the performance of R_4Sb_3 compounds, contributing to the development of advanced materials for thermoelectric energy conversion.

Introduction

With today's challenging worldwide energy needs, efficient waste heat recovery via thermoelectric energy conversion is very attractive. Nonetheless, the choice of thermoelectric generation rather than another method for producing electrical energy is driven by a number of factors. Cost, conversion efficiency, reliability, type and temperature of heat source and heat sink, weight, size, and other variables need to be carefully considered. However, the remarkable properties of thermoelectric generators are unique. Given how easy this technology can be incorporated in a wide range of waste energy streams, from automobile exhaust gas to industrial waste heat associated with manufacturing processes like forming and melting, the benefits at stake are enormous.

While commercial thermoelectric materials are available for low (below 400 K) and medium temperatures (between 400 and 800 K), high-temperature (above 800 K) thermoelectric materials are only very rarely commercially accessible. Such materials are required for limited but important applications, for instance in spacecraft. Indeed, such a temperature range is not manageable by modules made of the classical magnesium or manganese silicides, or skutterudites thermoelectric compounds for instance. Currently, both n- and p-type SiGe,[1] the p-type Zintl phases $Yb_{14}MnSb_{11}$ [2] and $Yb_{21}Mn_4Sb_{18}$,[3] some Half-Heusler compounds [4] as well as some rare-earth metal antimonides or tellurides are among the scarce promising candidates for the development of high temperature thermoelectrics. Among the latter, *n*-type $La_{3-x}Te_4$ which adopts a defect thorium phosphide Th_3P_4 crystal structure, with vacancies on the rare-earth sites exhibits a zT above the unity around 1300 K.[5] Somewhat related compounds that crystallize in the anti-Th_3P_4 structure, may also be potential candidates for high-temperature thermoelectric applications: This is notably the case for R_4Sb_3 compounds (R = La, Yb, Ce, Sm).[21] Interestingly, experimentally measured Seebeck coefficients show a difference in behaviour for Yb_4Sb_3 compared to the three other binary compounds, increasing upon the temperature and showing p-type conduction properties, whereas all the three other compounds are rather n-type semi-conductors and showcase slightly decreasing Seebeck values upon temperature increasing. Even if Yb_4Sb_3 resistivity increases linearly with the temperature, which suggests a metallic-like behaviour, the encouraging Seebeck values measured for the compound (up to 70 μV/K at 1000°C) makes it a really interesting candidate for high-temperature applications, and raises interrogations about its differences with the other compounds of the series. It turns out that only a few studies have been carried out over the years in order to see

how to enhance (or not) the thermoelectric properties of Yb_4Sb_3.[6,25,25] We have ourselves recently shown experimentally that doping with one or two additional atomic elements significantly decreases the thermal conductivity but only slightly improves the thermopower, leading to a maximum *zT* value of 0.5 at 1300 K.[25,25]

To complete our studies, we carried out a theoretical study using density functional theory calculations (DFT) aiming to explain the differences in the bonding and transport properties between Yb_4Sb_3 and La_4Sb_3. A special attention was paid to the analysis of the bonding using the Crystal Orbital Bond Index (COBI) recently developed in the group of R. Dronskowski,[11] showing a more ionic character of the former with respect to the latter. To support our conclusions, a comparison was made with the chemical bonding of the isostructural Ba_4Q_3 (*Q* = Sb, Bi) 'ionic' compounds. We report in this article, the main results on the electronic structure analysis in these compounds and we discuss the consequences on their structural and transport properties.

Computational details

The based-DFT *VASP* code (version 6.2.0) was used for geometry optimizations and band-structure calculations.[7] The generalized gradient approximation (GGA) was used to describe the exchange-correlation (XC) interaction, and the parametrization of Perdew, Burke and Ernzerhof (PBE) was employed.[8] Projector-augmented wave potentials were used for all atoms.[9] Calculations were performed using a cut-off energy of 350 eV. The Monkhorst-Pack method was used to sample the irreducible Brillouin zone for the calculations of the electronic wave-functions, and no symmetry constraints were considered for the optimization of the cell parameters and atomic positions.[10] Chemical bonding analyses of plane-wave data by COBI[11] and atomic charges were performed using the *LOBSTER* (version 5.1.0) code.[12] COBI is a new quantity that defines the nature of the bonds based on the bond index of Wiberg and Mayer adapted for the crystals. The qualitative and quantitative interpretations of COBI closely resemble the more familiar crystal orbital overlap population (COOP) and crystal orbital Hamiltonian populations (COHP),[13,14] and directly relates to the classical bond order. Density of states (DOS) and COBI plots were drawn by with the WxDragon program.[15] The *VASPKIT* program was also used for post-processing of the *VASP* calculated data.[16] Band structures, DOS, and crystal orbital Hamiltonian population (COHP) curves were shifted in such a way that the Fermi level lies at 0 eV.

Results and Discussion

R_4Sb_3 (R = La, Yb, Sm, Ce) compounds crystallize in the anti-Th_3P_4 structure (space group $I\bar{4}3d$, no. 220). The Th_3P_4 structure adopts a cubic structure in which Th atoms (Wyckoff position 12*a*) are located in the middle of a square-based antiprism, whereas P atoms (Wyckoff position 16*c*) are surrounded by Th atoms forming an octahedron.[17] In the case of rare-earth antimonides, rare-earth atoms occupy the P sites, whereas antimony atoms occupy the Th sites (Fig. 1). Distortions of the square-based antiprisms and octahedra are observed: Rare-earth atoms are bonded with Sb atoms via three short and three long bonds (Table 1). For La_4Sb_3 the shortest La–La contacts are comparable to the one found in the hcp La structure (3.733Å). In the case of Yb_4Sb_3, Yb–Yb contacts are significantly shorter (3.560 Å) than the one encountered in ccp Yb metal (3.876 Å).

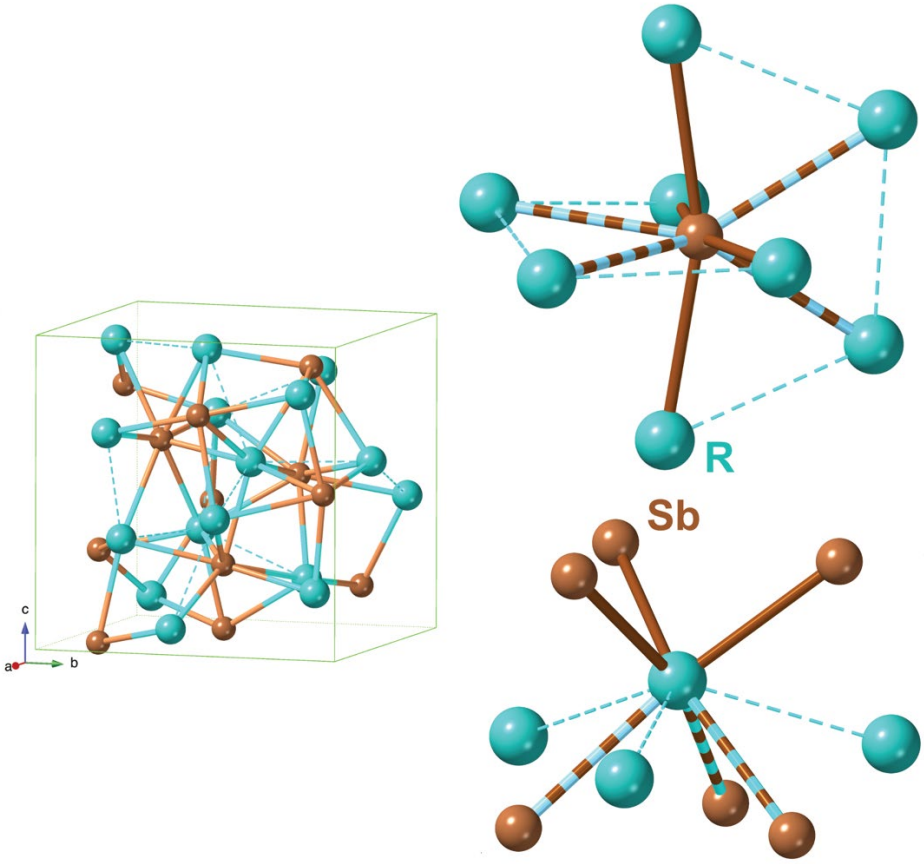

Fig. 1. Crystal structure of R_4Sb_3: Unit cell (left) and atomic environments (right). In the latter, short and long R–Sb contacts are shown with brown and alternate brown/blue colours, respectively. The contacts between neighbouring rare-earth atoms and antimony atoms are not shown in the bottom right figure.

Table 1. DFT optimized structural parameters of R_4Q_3 (*R* = La, Yb, Ba; *Q* = Sb; Bi) compared with available X-ray ones.

Compound	La_4Sb_3		Yb_4Sb_3		Ba_4Sb_3	Ba_4Bi_3	
	X-ray[18]	DFT	X-ray[19]	DFT	DFT	X-ray[22]	DFT
a (Å)	9.649	9.704	9.322	9.378	10.561	10.550	10.743
R–Sb (Å)	3.211	3.232	3.134	3.139	3.528	3.536	3.590
	3.476	3.494	3.323	3.359	3.789	3.772	3.853
R–R (Å)	3.720	3.739	3.560	3.596	4.056	4.040	4.125

Bonding analysis of La_4Sb_3

Total atom- and orbital-projected density of states (DOS) computed for La_4Sb_3 are sketched in Fig. 2. It is consistent with the band structure previously computed by Takegahara *et al*. for this compound.[20] A pseudo-band gap of about 0.25 eV width separates the valence band from the conduction band. The Fermi level crosses the bottom of the latter. The conduction band is mainly centred on lanthanum *d* levels; the antinomy levels hardly contributing to these bands. On the contrary, the top of the valence band is based on La and Sb atoms: the *p* levels of Sb contribute the most whereas the contribution of the *d* orbitals of La is the second most important. Most of *f* levels of lanthanum are lying above the Fermi level, as expected for a trivalent La^{3+}.

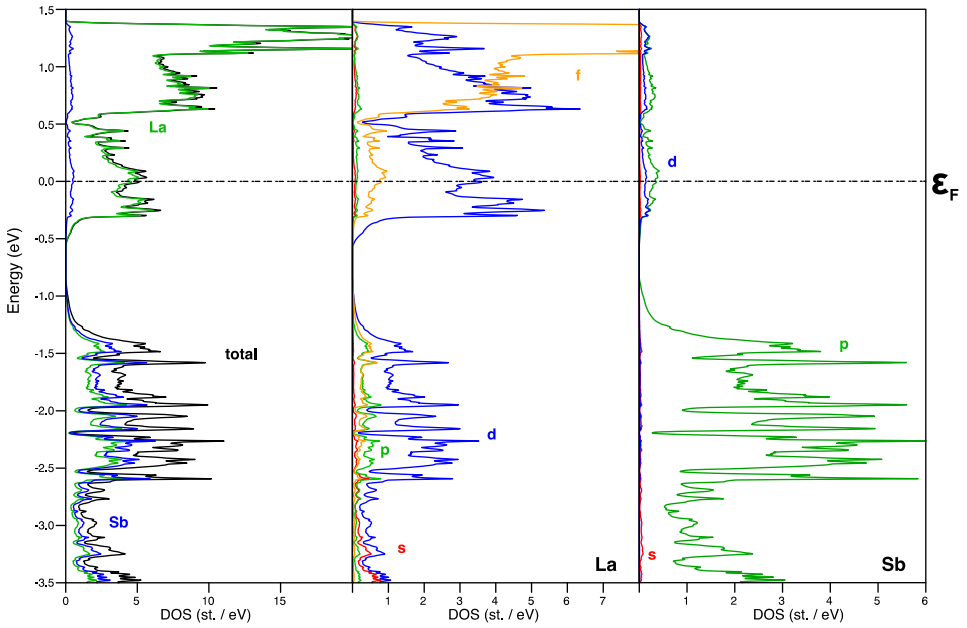

Fig. 2. Total, atom and orbital-projected DOS computed for La_4Sb_3.

The crystal orbital bond index (COBI) was used in the context of bond order and degree of covalency in La–La and La–Sb contacts (Fig. 3).[11] The bond orders are approximated using the integrated COBI (ICOBI) values that are dimensionless. A 'perfect' covalent bond is shown by an ICOBI index that has a very close value of one whereas the 'perfect' ionic bond exhibits an index close to zero. La–Sb COBI curves shows positive contributions in the valence band and negative ones in the conduction band. This is expected since La-d–Sb-p bonding interactions are anticipated in the valence band. As expected from the COBI curves, the computed ICOBI values are larger for the short La–Sb contacts (0.46 for 3.232 Å) than for the long La–Sb ones (0.28 for 3.494 Å). If these values suggest that ionic interactions predominate over the covalent ones between the rare-earth and pnictogen atoms in this structure, computed Löwdin charges (–0.49 and 0.37 for Sb and La atoms, respectively) are far from the idealized Zintl-Klemm charges and reflect a significant covalent character of La–Sb bonds in this compound. The conduction band shows a significant positive contribution to La–La contacts. Occupation of the bottom of the conduction band leads to an ICOBI value of 0.15 for La–La. As a comparison, an ICOBI value of 0.25 is computed in La metal. Note that the computed ICOHP values are equal to –1.2 eV/cell for La–La contacts (to be compared to the ICOHP of –1.46 and –0.88 eV/cell computed for short and long La–Sb contacts, respectively) confirm rather strong metal–metal interactions in La_4Sb_3.

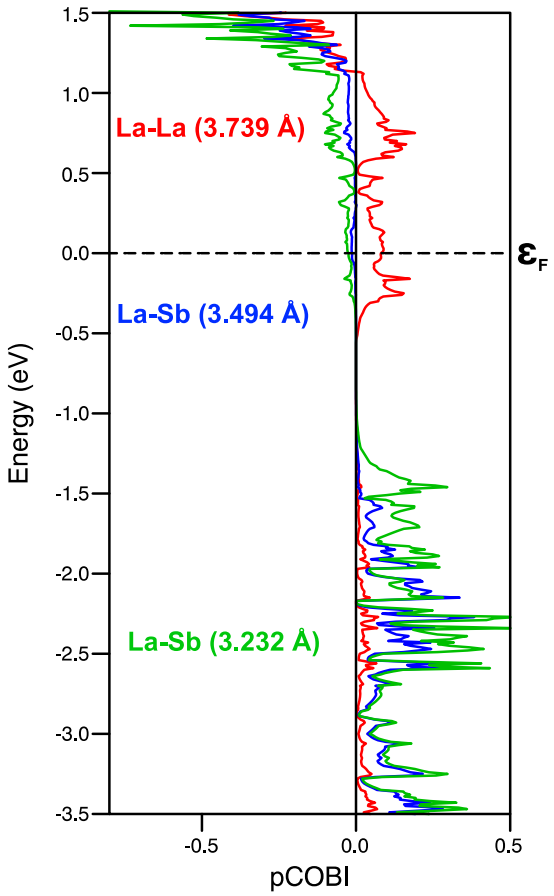

Fig. 3. COBI computed for various contacts in La_4Sb_3.

How does Yb_4Sb_3 compare?

The thirteen additional electrons of the free Yb atom with respect to the free La atom mainly occupy the 4*f* orbitals and its ground state electronic configuration is $[Xe].4f^{14}.6s^2$. This leads to the two possible +2 and +3 oxidation states in solid-state compounds. A magnetic state being reported for Yb_4Sb_3, spin-polarized calculations were carried out. A magnetic moment of 1.28 µB per unit cell was computed. This is rather close to the one resulting from magnetic susceptibility experiments,[21] that leads to an effective moment of 0.39 µB per Yb (giving the value of 1.56 µB per unit cell which contains 4 Yb atoms). It is noteworthy that the integration of spin-orbit coupling in the GGA calculations decreases the magnetic moment per unit cell to 0.81 µB. These values suggest that Yb^{2+}, that presents an effective moment equal to 0, is mainly present in the compound to the detriment of Yb^{3+} – which has a magnetic moment of 4.54 µB.

Fig. 4 shows the total and different projections of the spin-polarized DOS computed for Yb_4Sb_3. The small differences between both spin contributions are consistent with the weak magnetic moment computed for the compound. The Fermi level crosses a DOS peak mainly centred on *f* levels of Yb. This DOS peak presents also a minor contribution from *d* orbitals of Yb and *p* orbitals of Sb. Similarly to La_4Sb_3, the bands lying between –4 and –0.5 eV are almost equally distributed on Yb and Sb levels whereas those lying above 1 eV are mainly centred on Yb. The position of 4*f* levels is the main difference in the electronic structure of La_4Sb_3 and Yb_4Sb_3: in the former, they are lying in the conduction band, mainly above +0.5 eV, whereas in the latter, they are lying in the vicinity of the Fermi level and occupied.

The COBI curves have been computed for the shortest Yb–Sb and Yb–Yb contacts in Yb_4Sb_3. Since spin-polarization is weak and for the sake of clarity, spin contributions to COBI were averaged (Fig. 5). Negative contributions to COBI are computed for all contacts in the conduction band. Below –0.5 eV, positive contributions to COBI are computed for Yb–Sb contacts; COBI computed for Yb–Yb contacts are almost null for these bands. The DOS peak crossed by the Fermi level show negative contributions to COBI for Yb–Sb contacts. COBI for Yb–Yb contacts reaches 0.1 at the bottom of this DOS peak. It decreases with the increase of energy and becomes negative around –0.15 eV. It is noteworthy that the range of COBI curves is much smaller for Yb_4Sb_3 (between –0.1 and 0.1] in the energy range between –4.0 and 1.5 eV) compared to La_4Sb_3 (between –0.5 and 0.4] in the same energy range). This suggests that the covalent character is largely weaker in Yb_4Sb_3 compared to La_4Sb_3. ICOBI values are consistent with this statement since they are equal to 0.07 and 0.05 for short (3.159 Å) and long (3.359 Å) Yb–Sb contacts, respectively – to be compared to 0.46 and 0.28 for the corresponding La–Sb contacts). Additionally, the computed ICOBI for Yb–Yb contacts (0.01) suggests weak ionic interactions between metal atoms in this compound. Computed Löwdin charges of +1.45 and –1.93 for Yb and Sb, respectively indicate also that ionic interaction plays a more important part in the bonding in Yb_4Sb_3 compared to La_4Sb_3 +0.37 and –0.49 for La and Sb, respectively, see above).

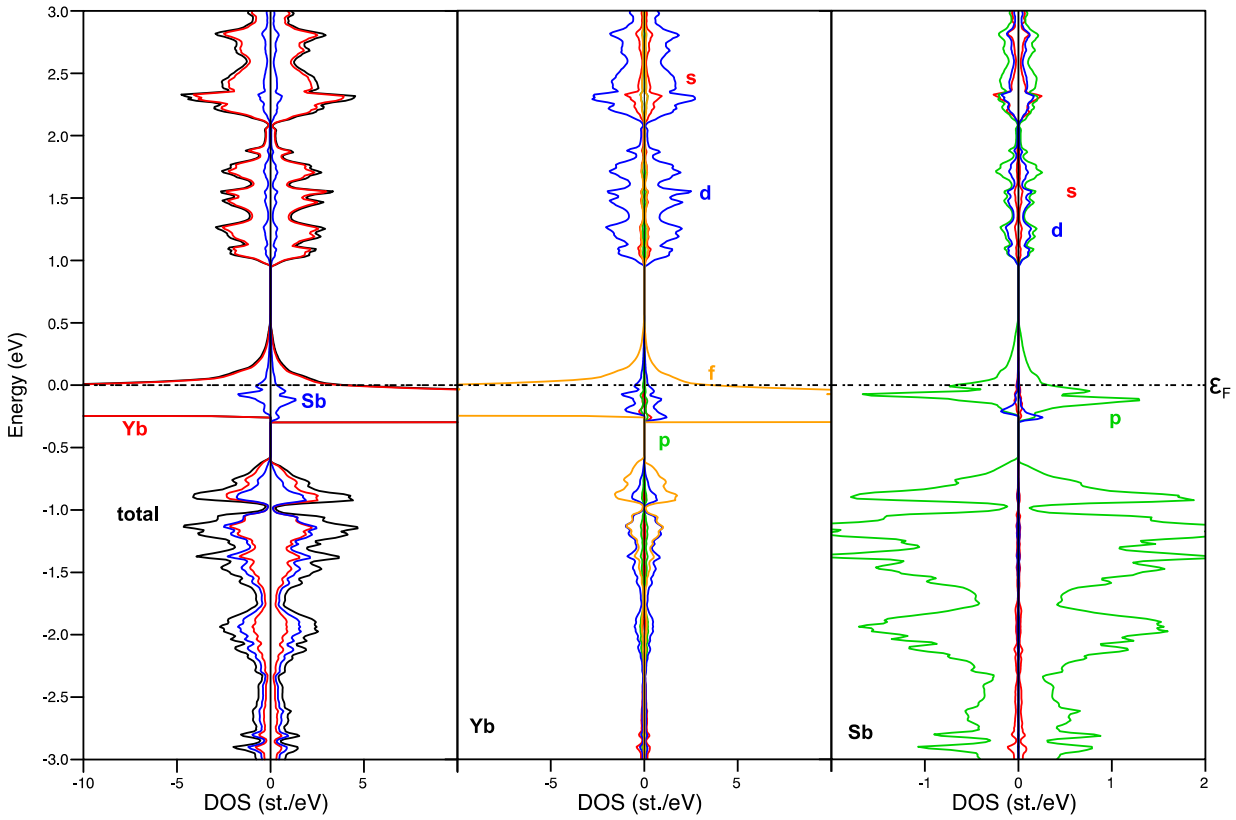

Fig. 4. Total, atom and orbital-projected spin-polarized DOS computed for Yb_4Sb_3.

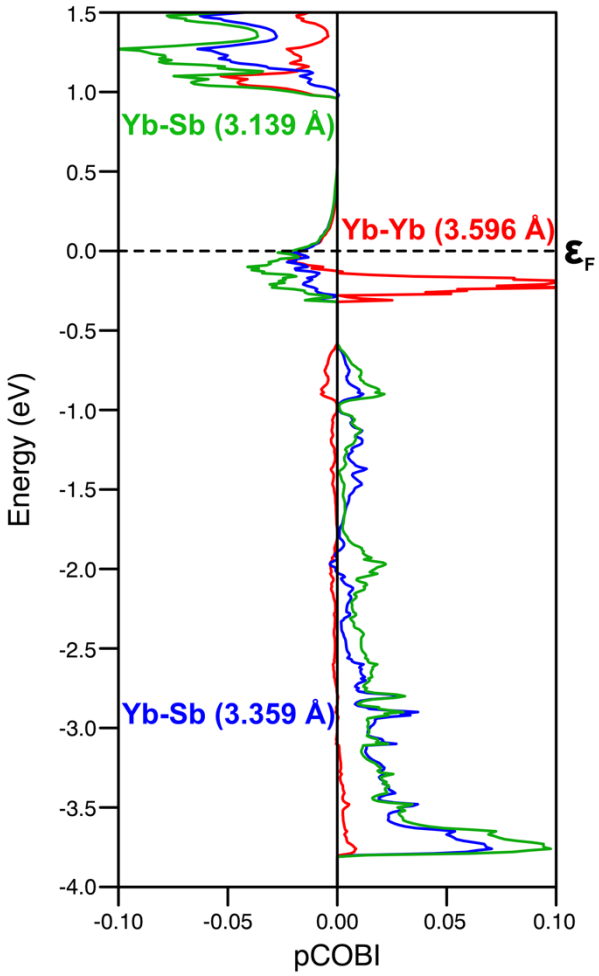

Fig. 5. COBI computed for various contacts in Yb_4Sb_3.

Electronic structure of Ba_4Q_3 (Q = Sb, Bi) analogues

In 2003, Corbett *et al.* synthesized Sr_4Bi_3 and Ba_4Bi_3 that both adopt the same anti-Th_3P_4 crystal structure as R_4Sb_3.[22] Resistivity measurements showed that Ba_4Bi_3 is a good metallic conductor as well as the isostructural Eu_4Bi_3 compound. The latter was shown to exhibit Eu^{2+} according to previous magnetic susceptibility measurements.[23] Tight-binding LMTO-ASA DFT calculations showed that the band structures of Sr_4Bi_3 and Ba_4Bi_3 are quite similar and agree with their metallic properties. The calculations of COHP for Sr–Bi contacts confirm the Sr–Bi bonding character of the valence band and the Sr–Bi antibonding character of the conduction band.[ref] We carried out DFT calculations on Ba_4Bi_3 and Ba_4Sb_3 compounds, thinking that even if the latter is hypothetical, it was interesting to compare its electronic structure with its bismuth analogue and the rare-earth antimonides as well. DFT-optimized cell parameters and bond distances are reported in Table 1. In

the case of Ba_4Bi_3, they compare rather well with the ones resulting from a previous X-ray diffraction study.[22] The use of PBE functional leads to a slight overestimation of *ca.* 2-3% of the structural parameters as often observed with this GGA XC functional. Barium atoms are bigger than ytterbium ones according to their atomic radii. Therefore, it is expected that the unit cells of Ba_4Q_3 compounds are larger than that of the rare-earth analogues (Table1). Ba–Sb contacts are about 0.4 Å longer than R–Sb contacts (*R* = La, Yb). Ba–Bi contacts are less than 0.1 Å longer than Ba–Sb as expected from the respective radii of Bi and Sb.

The DOS computed for Ba_4Sb_3 is sketched in Fig. 6 as well as COBI curves for shortest Ba–Sb and Ba–Ba contacts. The Fermi level crosses the top of the valence band which is separated from the conduction band by a gap of *ca.* 0.9 eV. As for R_4Sb_3 (*R* = La, Yb), the conduction band is mainly centred on Ba whereas the valence band is dominated by Sb. The bands that lie between –1.8 and 0.5 eV exhibit positive contributions to Ba–Sb contacts whereas the conduction band shows negative contribution to these contacts. It is noteworthy that Ba–Ba COBI is not significant in the bands that lie below 0.5 eV. The Ba–Ba ICOBI is equal to 0.03, a value similar to that computed for Yb–Yb contacts in Yb_4Sb_3. ICOBI values of 0.13 and 0.09 are computed for short (3.529 Å) and long (3.789 Å) Ba–Sb distances. These values are only slightly higher than those computed for Yb_4Sb_3. As for Yb_4Sb_3, all ICOBI values suggest predominant ionic interatomic interactions in this hypothetical Ba_4Sb_3. Note that DOS and COBI curves computed for Ba_4Bi_3 show strong similarities with the ones computed for Ba_4Sb_3 (Fig. S1). Finally, computed Löwdin charges are equal in both compounds: +1.43 and –1.91 for Ba and Q (*Q* = Sb, Bi), respectively, and almost identical to those computed for Yb_4Sb_3 (vide supra).

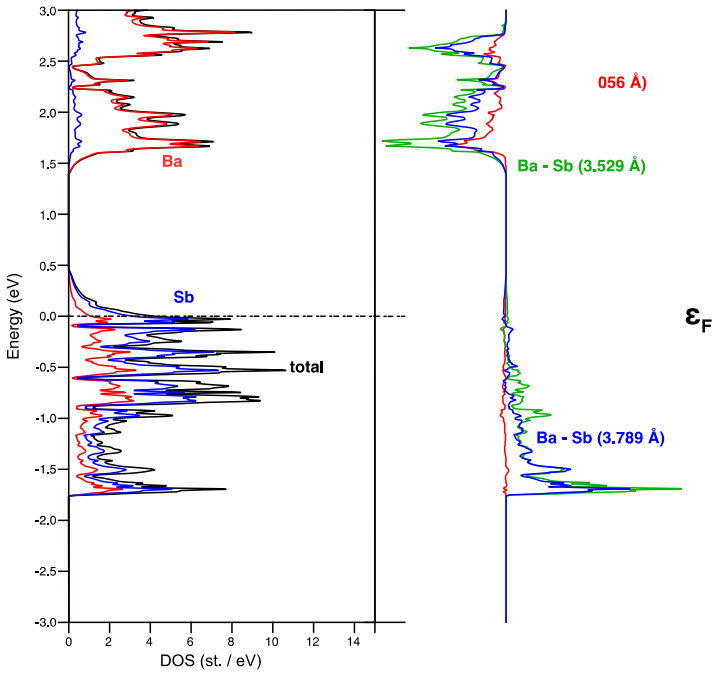

Fig. 6. Total and atom-projected DOS, and Ba–Sb and Ba–Ba COBI computed for Ba_4Sb_3.

Discussion

In the light of these results, one can have a look at the transport properties of rare-earth R_4Sb_3 and related compounds. The analysis of the electronic structure of these compounds showed that one major difference between Yb_4Sb_3 and La_4Sb_3 lies in the position of the Fermi energy in the band structure. Since the Fermi level of La_4Sb_3 lies in the conduction band, electrons are expected to dominate its electronic transport properties. This is consistent with the negative thermopower measured for La_4Sb_3. In the case of Yb_4Sb_3, the bonding analysis revealed that the divalent oxidation state of ytterbium prevails. Then, the electronic structure of this compound gets closer to that of the isostructural Ba_4Q_3 (Q = Sb, Bi) compounds than the trivalent rare-earth analogues. In barium pnictides analogues, the Fermi level crosses the top of the valence band suggesting that holes will govern the electronic transport properties in these compounds. The measurement of the thermopower of Yb_4Sb_3 as a function of temperature showed that it is also the case above *ca.* 500 K.[21,24] Below this temperature, the Seebeck coefficient is measured negative. Such a behaviour suggests that several bands are involved in the electronic transport properties of Yb_4Sb_3. This is confirmed by the spin-polarized band structure recently published for this compound.[24] Two bands

crossed by the Fermi level along the Γ → N → P → Γ → H symmetry directions and two others in the H → N directions are expected to play some role in the electronic transport properties.

The DOS computed for R_4Sb_3 (*R* = La, Yb) sketched in Figs. 2 and 4, respectively, suggest that semiconducting properties can be envisioned for these compounds. Assuming a rigid band model, this can be achieved for specific charge carrier concentrations for both compounds. Doping these phases is a common way to reach this goal: Yb_3LaSb_3 compound with anti-Th_3P_4 structure and the following charge distribution $(Yb^{2+})_3(La^{3+})(Sb^{3-})_3$ should behave as a semiconductor. In 2010, Chamoire *et al.* reported doping of Yb_4Sb_3 with La and Sm: $Yb_{4-x}R_xSb_3$ phases were synthesized with maximum *x* values equal to 0.5 and 0.4 for La and Sm, respectively.[21] Recently, we studied the co-doping of Yb_4Sb_3 with Ce and Bi.[25] Results showed that the solubility limit *x* of Ce is equal to 0.4 in $Ce_xYb_{4-x}Sb_{2.8}Bi_{0.2}$. This year, we demonstrated that the compositions of $La_xYb_{4-x}Sb_{2.8}Bi_{0.2}$ with $x > 0.3$ display LaSb impurities and exhibit distorted peaks in their X-ray diffraction diagrams.[24] All these experimental results confirm that substitution of ytterbium with trivalent rare-earth atoms in Yb_4Sb_3 is limited to a value of around 10%. Although such a limitation is unexpected since isostructural rare-earth binaries have been synthesized, our theoretical analysis demonstrates that the chemical bonding properties are different in divalent compounds such as Yb_4Sb_3 and trivalent ones such as the lanthanum analogue. This may be at the origin of the limited doping of Yb_4Sb_3 with rare-earth trivalent atoms that restricts the potential optimization of its electronic transport properties.

Conclusions

In summary, this study provides significant insights into the electronic structure and bonding characteristics of rare-earth antimonides, particularly Yb_4Sb_3 and La_4Sb_3, and their potential for high-temperature thermoelectric applications. Through DFT calculations and chemical bonding analyses, it was demonstrated that Yb_4Sb_3 exhibits predominantly an ionic character with divalent ytterbium, contrasting with the more covalent bonding in La_4Sb_3. This difference in bonding and electronic structure impacts their respective transport properties, with Yb_4Sb_3 showing p-type conduction at high temperatures, while La_4Sb_3 remains an n-type conductor. The study also highlights the challenges in doping Yb_4Sb_3 with trivalent rare-earth atoms, which may limit the optimization of its thermoelectric properties. These findings contribute to a better understanding of

these compounds and their applicability in waste heat recovery and other high-temperature applications.

Author contributions

We strongly encourage authors to include author contributions and recommend using CRediT for standardised contribution descriptions. Please refer to our general author guidelines for more information about authorship.

Conflicts of interest

In accordance with our policy on Conflicts of interest please ensure that a conflicts of interest statement is included in your manuscript here. Please note that this statement is required for all submitted manuscripts. If no conflicts exist, please state that "There are no conflicts to declare".

Data availability

A data availability statement (DAS) is required to be submitted alongside all articles. Please read our full guidance on data availability statements for more details and examples of suitable statements you can use.

Acknowledgements

The authors are grateful to the Agence Nationale de la Recherche (ANR – Project HIGHTHERM – ANR-18-CE05-0037). V.P. thanks the Région Bretagne for a Ph.D. grant.

Supporting Information

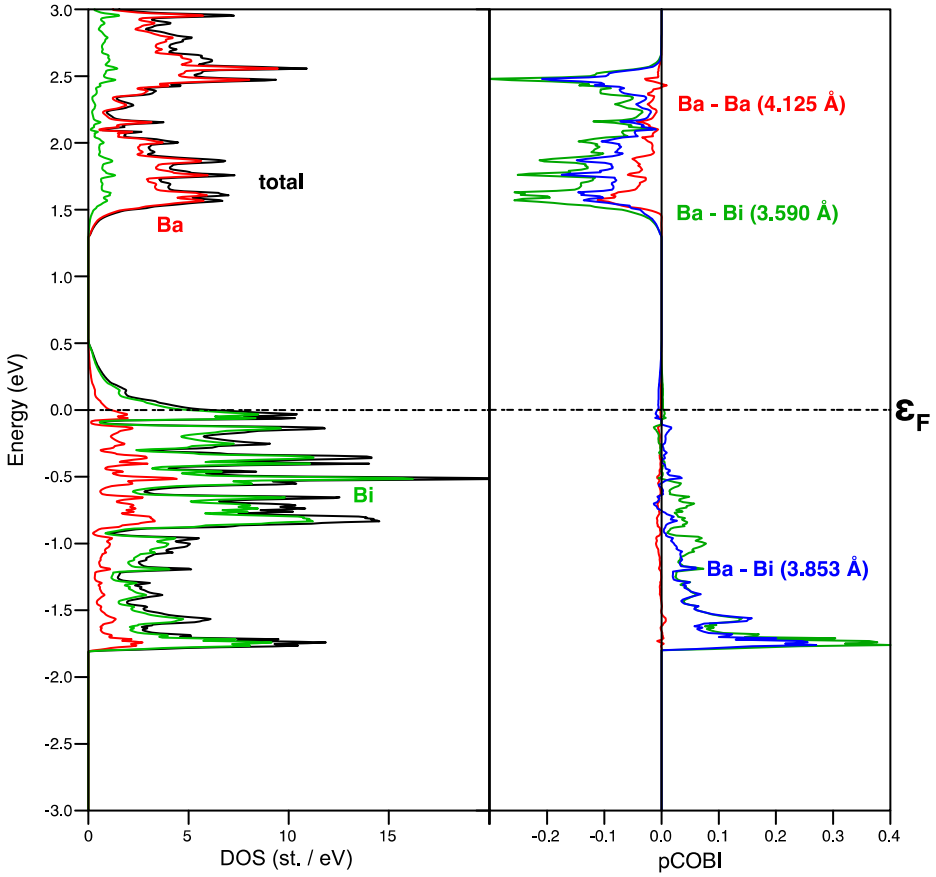

Fig. S1. Total and atom-projected DOS, and Ba–Bi and Ba–Ba COBI computed for Ba_4Bi_3.

References

[1] B. Cook, *Energies*, 2022, **15**, 2957.

[2] S. R. Brown, S. M. Kauzlarich, F. Gascoin and G. J. Snyder, *Chem. Mater.*, 2006, **18**, 1873–1877.

[3] A. He, S. K. Bux, Y. Hu, D. Uhl, L. Li, D. Donadio and S. M. Kauzlarich, *Chem. Mater.*, 2019, **31**, 8076–8086.

[4] J. W. G. Bos, in Thermoelectric Energy Conversion, ed. R. Funahashi, Woodhead Publishing, 2021, pp. 125–142.

[5] (a) A. May, J.-P. Fleurial and G. J. Snyder, *Chem. Mater.,* 2010**, 22**, 2995; (b) A. May, J.-P. Fleurial and G. J. Snyder, *Phys. Rev. B,* 2008, **78**, 125205.

[6] A. Chamoire, R. Viennois, J.-C. Tedenac, M. M. Koza, F. Gascoin, *J. Elec. Mater.*, 2011, **40**, 1171–75.

[7] (a) G. Kresse and J. Furthmüller, *Comput. Mater. Sci.*, 1996, **6**, 15—50; (b) G. Kresse and J. Furthmüller, *Phys. Rev. B: Condens. Matter Mater. Phys.*, 1996, **54**, 11169—11186.

[8] J. P. Perdew, K. Burke and M. Ernzerhof, *Phys. Rev. Lett.*, 1996, **77**, 3865–3868.

[9] (a) P. E. Blöchl *Phys. Rev. B: Condens. Matter Mater. Phys.*, 1994, **50**, 17953—17979; (b) G. Kresse and D. Joubert, *Phys. Rev. B: Condens. Matter Mater. Phys.*, 1999, **59**, 1758—1775.

[10] H. J. Monkhorst, J. D. Pack, *Phys. Rev. B,* 1976, **13**, 5188–5192.

[11] P. C. Müller, C. Ertural, J. Hempelmann and R. Dronskowski, *J. Phys. Chem. C,* 2021, **125**, 7959–7970.

[12] (a) S. Maintz, V. L. Deringer, A. L. Tchougréeff, R. Dronskowski, *J. Comput. Chem.,* 2016, **37**, 1030–1035; (b) S. Maintz, M. Esser and R. Dronskowski, *Acta Phys. Pol. B,* 2016, **47**, 1165—1175; (c) R. Nelson, C. Ertural, J. George, V. L. Deringer, G. Hautier and R. Dronskowski, *J Comput. Chem.*, 2020, **41**, 1931–1940.

[13] R. Dronskowski and P. E. Blöchl, *J. Phys. Chem.*, 1993, **97**, 8617—8624.

[14] V. L. Deringer, A. L. Tchougreeff and R. Dronskowski, *J. Phys. Chem. A,* 2011, **115**, 5461—5466.

[15] B. Eck B. wxDragon 2.2.3. Aachen, Germany: RWTH Achen University, 2020.

[16] V. Wang, N. Xu, J.C. Liu, G. Tang and W.T. Geng, *Comput. Phys. Comm.*, 2021, **267**, 108033

[17] K. Meisel *Z. Anorg. Chem.*, 1939, **240**, 300–312.

[18] Y. Wang, L. D. Calvert and J. B. Taylor, *Acta. Crys. B.,* 1980, **36**, 221–222.

[19] A. Ochiai, T. Suzuki and T. Kasuya, *J. Phys. Soc. Japan,* 1990, **59**, 4129–4141.

[20] K. Takegahara, H. Harima and T. Kasuya, *J. Magn. Magn. Mater.*, 1985, **52**, 0307–309.

[21] A. Chamoire, F. Gascoin, C. Estournès, T. Caillat and J.-C. Tédenac, *Dalton Trans.,* 2010, **39**, 1118–1123.

[22] B. Li, A.-V. Mudring and J. D. Corbett, *Inorg. Chem.*, 2003, **42**, 6940–45.

[23] M. E. Wang, J. T. Chang and S. M. Kauzlarich, *Z. Anorg. Allg. Chem.*, 1996, **622**, 432–436.

[24] H. Bouteiller, V. Pelletier, S. Le Tonquesse, B. Fontaine, T. Mori, J.-F. Halet, R. Gautier, D. Berthebaud and F. Gascoin, *Mater. Adv.*, 2024, **5**, 1217–1225.

[25] S. Le Tonquesse, H. Bouteiller, Y. Matsushita, A. Cortez, S. K. Bux, K. Imasato, M. Ohta, J.-F. Halet, T. Mori, F. Gascoin, D. Berthebaud, *ACS Appl. Energy Mater.,* 2023, **6**, 10088–10097.